 SDHM, vol.6, no.3, pp.123-160, 2010

# Facts and Effects to be Considered when Validating 2D and 3D UD Composite Failure Conditions – experiences from participation in the World-Wide-Failure-Exercise

**R. G. Cuntze**[1]

**Abstract:** The paper deals with the validation of 2D and 3D failure conditions of unidirectional (UD) composites composed of endless fibres and thermoset matrices. The generation of these failure conditions is shortly described and then applied to test cases of the World-Wide-Failure-Exercises WWFE-I and II, organized by Qinetic in the past 20 years. The derivation of the conditions for the brittle fracture failure experiencing UD lamina material was based on the author's so-called Failure Mode Concept (FMC) which basically builds up on the hypotheses of Beltrami and Mohr-Coulomb. The generally applicable FMC is applied here to UD material. Essential topics of the paper are specific facts and effects to be considered when validating. This includes 'global fitting' versus 'failure mode fitting' and some test specifica.
As conclusions can be drawn from the investigations: 1. The FMC is an efficient concept because it very *strictly* utilizes a 'thinking in failure modes' as well as the consideration of *material symmetry* aspects. It has proven to be a helpful tool in simply fitting the course of multi-axial UD strength test data, and it can capture several failure modes in one final 'global' effort equation; 2. The validation was partly successful, sometimes first after re-evaluation of test data provided by Qinetic. A full 2D and 3D validation can be not yet achieved due to some still missing test data and some shortfalls in the experiments.

**Keywords:** Failure conditions, brittle UD laminae, 2D/3D validation, test data quality

## 1 Introduction

A failure condition is the mathematical formulation of a failure curve or of a failure surface. Failure conditions are necessary for Design Verification. Static design ver-

[1] Prof. Dr.-Ing. habil. Ralf G. Cuntze, formerly MAN Technologie AG, Augsburg, Germany; D-85229 Markt Indersdorf, Tel. & Fax: 0049 8136 7754, E-mail: Ralf_Cuntze@t-online.de

ification has to be performed for *onset of fracture*. The brittle behaving UD material requires failure conditions which are fracture conditions. Failure conditions assess a multi-axial stress state which acts in the critical material 'point' by utilizing just one uni-axial strength $R$ and, hopefully to make it simple, an equivalent stress $\sigma_{eq}$ representing the multi-axial stress state. In the validation to be performed here, the strength failure of non-cracked structural parts is addressed only which means *material strength failure*. Stability failure as a *structural strength failure* has to be avoided in the test because associated test data cannot be used for validation.

The FMC is based – as far as material homogenization permits to do it - on material symmetry-related invariants, which have proven to be a helpful tool in simpler fitting multi-axial strength test data. The FMC enables to simply capture several failure modes in one equation, but without the short-comings of classical global conditions, i.e. Drucker-Prager for isotropic material and Tsai-Wu for UD material.

In the WWFE, *failure theories* are tested. Such a failure theory is composed of three parts, at least: 1) The *failure conditions* to assess tri-axial states of stress; 2) Non-linear stress-strain modelling of the embedded UD lamina material (in strain-hardening and strain-softening regime as main degradation domain) as analysis input; and 3) Non-linear coding for obtaining a realistic response of lamina and laminate test specimens considering possible changes of the fibre direction under loading. 4) In the WWFE-II, in addition to WWFE-I one more point is to be regarded: Modelling of the matrix behaviour in ultra-high pressure domains.

In consequence, the validation of a failure condition is just one part of a failure theory exercise. This has to be considered when judging just the failure conditions of the competing WWFE contributors. Validation of UD failure conditions (point 1) is performed best with sets of multi-axial UD lamina strength test data, and approximately with laminate test data. Later, the laminates have to deliver valuable benchmarks.

The following questions of A.S. Kaddour from Qinetic describe the objectives of the WWFE: "*1) How well can current theories predict failure in FRP Composites?; 2) What are the boundaries of applicability of current design methodologies?; 3) Do composite designers have the right and accurate tools?; 4) Will virtual testing become a reality?"*

Whereas WWFE-I was attributed to 2D-problems WWFE-II deals with 3D stress states. Qinetic formulates the aims of the WWFE-II as: "*Solve specific gaps identified in WWFE-I. Identify well established champions of (tri-axial) 3D failure criteria. Validate and benchmark their models. Identify any gaps in the current 3D models. Identify specific shortfalls in experimental data test results. Stimulate the composites community to provide better tools. Provide designers with guidance for*

*predicting accurate strength under 3D states of stress."*

Providing the contributors with a reliable test basis was the challenging task for the WWFE organizers from Qinetic, because proving the capability of the tri-axial FMC theory requires realistic, well evaluated, and well understood experimental data. Thereby it is presumed by the author: 1) Pore-free material, no layer waviness, edge effects do not exist; 2) Constant fibre volume content ($V_f = 60\%$); 3) Perfect bonding of the layers.

The Part A contributions represents the prediction whereas Part B displays a discussion of the provided data and finally the correlation theory-experiment. In this context shall be reminded: Fitting of usually not sufficiently large test data sets means mapping of an actual stochastic situation. Model parameters are variables. Therefore, a determined parameter is always attributed to such a specific actual case.

## 2 Short Derivation of the FMC-based UD Failure Conditions

### *2.1 Stress states, strengths and observed strength failure modes*

Fig. 1 depicts the 3D stress state $\{\sigma\} = (\sigma_1, \sigma_2, \sigma_3, \tau_{23}, \tau_{31}, \tau_{21})^T$ in a UD material cube. For completeness and general understanding it further depicts the 5 strengths in symbolic denotation, applied in the German guideline VDI 2014 to avoid misunderstanding in the application of material properties. In brackets, the US denotation is given. It may be seen that a quasi-isotropic plane exists (2-3 plane).

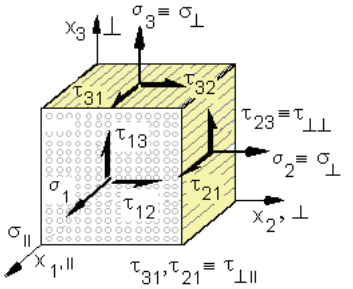


$$\{\sigma\}=(\sigma_1,\sigma_2,\sigma_3,\tau_{23},\tau_{13},\tau_{12})^T,$$

$$R_{\parallel}^{t}(=X^t), R_{\parallel}^{c}(=X^c), R_{\perp\parallel}(=S),\ R_{\perp}^{t}(=Y^t), R_{\perp}^{c}(=Y^c),$$

$$E_{\parallel}, E_{\perp}, G_{\parallel\perp}, \nu_{\perp\parallel}, \nu_{\perp\perp}$$

Figure 1: Transversely-isotropic material, 3D stress state.

Usual conventions are: Positive direction of the lamina orientation angle is from $x$ to fibre direction $x_1$; fibre in hoop direction of a tube means 90° to the axial direction. The indices t, c mean tension, compression, and $1 \equiv \parallel$ , $2 \equiv \perp$

The characterisation of the strength of transversely-isotropic composites (UD material) requires the measurement of five independent lamina strengths: $R^t_{||}$ and $R^c_{||}$ (tensile and compression strengths parallel to the fibres); $R^t_{\perp}$ and $R^c_{\perp}$ (tensile strength and compressive strength transverse to the fibre direction); and $R_{\perp||}$( shear strength, transverse/parallel to the fibre). The measurement of just these 5 strengths is standard. In practice, the strength in thickness direction is lower than the in-plane one, $\hat{R}^t_z < R^t_{\perp}$ . The real UD lamina is most often slightly orthotropic instead of being fully transversely-isotropic. UD thickness data are seldom provided.

Of interest for the establishment of material strength conditions is the number of strength failures observed in fracture tests. For the brittle UD lamina, fractography of test specimens reveals (Fig. 2, Masters (1994); Cuntze et al (1997)) that 5 fracture modes exist: 2 FF (Fibre Failure) + 3 IFF (Inter Fibre Failure).

Of highest importance for failure are the FF, however, the wedge failure mode IFF2 might be hazardous like an FF. Its criticality depends on stacking sequence and entire loading. Fig. 2 indicates also, that each single failure mode is governed by one single strength only.

*Note: In the following model validation or fitting or mapping of test data, respectively, average (typical) values for the strength parameters are required. These values are marked by a bar over.*

### *2.2 Modelling of UD material failure*

The FMC-based failure conditions addressed in this paper are most often termed strength criteria, however, the term condition is more accurate due to the fact that $F = 1$ is applied (F > = < 1 is termed failure criterion). They contain a minimum number of strength parameters as material symmetry is employed which is inherent to the chosen (homogenized) material model. Such a material model is an *ideal* model and can be treated as a crystal. However, to formulate a strength condition for a *real* material, there are physically missing parameters. These are the internal friction parameters $b_{\perp||}, b_{\perp\perp}$ of the UD material that are used in the FMC equations. These parameters are related to the corresponding friction properties as

$$b_{\perp||} = \mu_{\perp||}, \quad b_{\perp\perp} \cong 1/(1-\mu_{\perp\perp}). \tag{1a}$$

Friction properties can be measured in test, see Cuntze (2010a), via the measurement of the inclined fracture angle. Another method uses the $\sigma^c_2, \tau_{21}$ tests, and bi-axial tests($\sigma^c_2, \sigma^c_3$), Cuntze and Freund (2004):

$$b_{\perp||} = \frac{1 - \left(\tau^{\perp||}_{21}/\bar{R}_{\perp||}\right)^2}{2\sigma^c_2 \cdot \tau^{\perp||2}_{21}/\bar{R}^3_{\perp||}}, \quad b_{\perp\perp} = \frac{1 + (\sigma^c_2 + \sigma^c_3)/\bar{R}^c_{\perp}}{(\sigma^c_2 + \sigma^c_3)/\bar{R}^c_{\perp} + \sqrt{(\sigma^c_2 - \sigma^c_3)^2}/\bar{R}^c_{\perp}} \tag{1b}$$

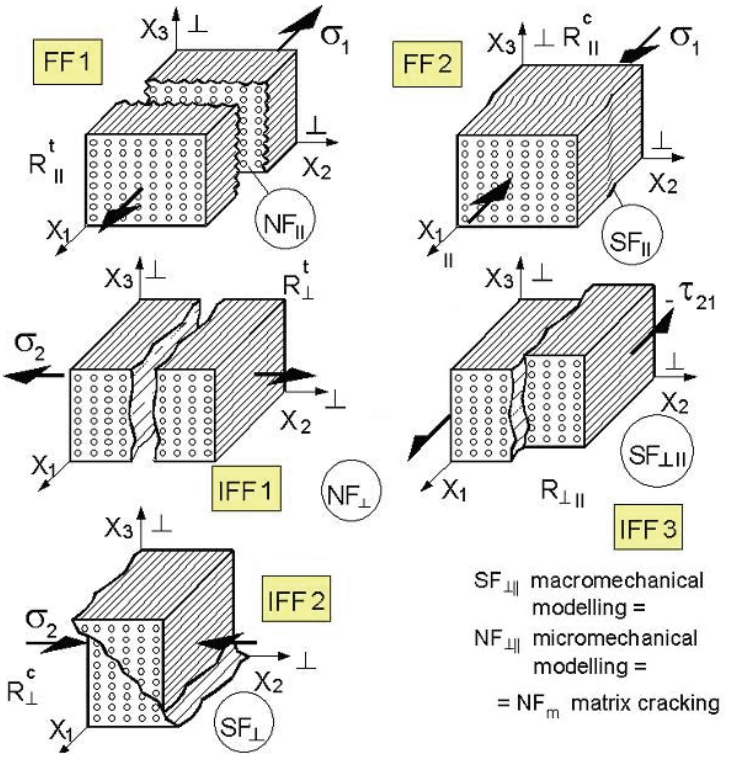


Figure 2: Scheme of fracture failure modes of UD material

Requirements for the development of failure conditions are:

- physically-based,
- simply formulated + numerically robust and
- just need the strengths (must be always available) for pre-dimensioning; further model parameters are assessable on the safe side
- condition shall be a mathematically homogeneous function.

Applying the FMC, Cuntze tries to formulate easy-to-handle homogeneous invariant-based failure conditions with stress terms of the lowest possible order. The conditions in mind shall be 'engineering-like' and shall not make a search of the fracture plane necessary which would be necessary when directly using a Mohr-Coulomb formulation.

The mathematical formulation of a failure condition is $F = 1$. *This can be interpreted as a material stress effort* $E_{ff}$ that reaches 100%. In the case of a global

formulation the condition has to capture several failure modes including all stresses and strengths. In contrast, the FMC includes the *mode active stresses* and just the single *mode-governing strength*.

Possibilities of formulating a failure condition are given by applying:

- stresses (strains have the disadvantage of neglecting residual stresses) or
- invariants (FMC employs such *stress* invariants).

Experience on isotropic and UD material shows, see Cuntze and Freund (2004); Cuntze (2004):

- Each of the observed fracture failure modes is linked to one strength;
- Material symmetry says: *Number of strengths = number of elasticity properties*
- Example UD material: $E_{||}$, $E_{\perp}$, $G_{||\perp}$, $\nu_{\perp||}$, $\nu_{\perp\perp}$. and
- Application of invariants for composites is also possible.

Formulations of strength failure conditions may follow, such as performed with Hashin/ Puck for unidirectional laminae, Mohr's postulate: "*Fracture is determined by the stresses in the fracture plane!"* This has a formulation advantage but makes the determination of the angle of the inclined fracture plane necessary. The failure condition is not scalar any more, e.g. the Hashin-Puck failure conditions in Puck (1996) or Puck and Schuermann (2002).

In the case of elasticities modelling a homogenization or 'smearing' is applicable for pre-assessment of elasticity properties whereas in case of strength modelling the smearing process may not be so effective due to the fact that, e.g. for UD, the micromechanical fibre strength $\sigma_{1f}$ determines fracture and not the macro-mechanical tensile stress $\sigma_1$, utilized in the lamina model.

Structural composites usually display brittle behaviour.

*Remark on the stress field in test specimen:* The critical material domain should not exhibit a stress concentration. In contrast, a smooth high stress domain shall be inherent in the test specimen associated with a low stress decay.

### *2.3 Short description of the FMC*

Due to the experience above the FMC postulates in its 'phenomenological engineering approach': Number of failure modes equals number of strengths! This means

for isotropic material 2 and for transversely-isotropic UD material 5 properties as well as 5 failure modes.

Reasons for choosing invariants when generating failure conditions are presented by Beltrami Beltrami (1885). He assumes: "*At 'onset of yielding' the material possesses a distinct strain energy density W". This is* composed of two portions (shown here for the simple isotropic case): the *dilatational energy* ($I_1^2$) and the *distortional energy* ($J_2 \equiv$ *'Mises'*) in $W \cdot 6E = (1-\nu) \cdot I_1^2 + (2+2\nu) \cdot J_2$ , wherein $E$ is the Young's modulus. The invariants $I_1^2$ describes the *volume* change of the cubic material element and $J_2$ its change of the *shape*. Both these changes can be witnessed by the fracture morphology. In order to formulate a relatively simple scalar failure condition one chooses as invariant a term that respects whether the cubic material element will experience a volume change in the considered mode or a shape change. The same idea is valid for UD material, Cuntze and Freund (2004); Cuntze (2004). In the case of brittle behaving materials one energy term is to be added, the friction energy, which is linked to a Mohr-Coulomb behaviour and requires the use of $I_1$.

In this way, from Beltrami, Mises (HMH), and Mohr/Coulomb (friction) may be derived "Each invariant term in the *failure function F* can be dedicated to one physical mechanism in the solid cubic material element", see Cuntze (2010a).

Therefore, the following foundations characterize the FMC:

- 1 failure mode represents 1 independent failure mechanism
- 1 failure condition represents 1 failure mechanism (interaction of stresses)
- 1 failure mechanism is governed by 1 strength.

New with the FMC is only:

- the strict thinking in failure modes,
- the individual interaction of a failure mode with the other modes by having no impact on another pure failure mode domain, and an
- a-priori physically-based reduction of the possibilities to formulate failure conditions.

The next chapter briefly lists all the derived failure conditions, see Cuntze (2010a,b).

### *2.4 Summary of the 3D FMC-based UD failure conditions*

The FMC enables to formulate an equivalent stress $\sigma_{eq}$ due to the fact that each failure mode is characterized by one strength, only. For each mode, analogously to

Mises Yielding can be written

$$E_{ff}{}^{mode} = \sigma_{eq}^{mode} / R^{mode}. \tag{2}$$

Eq.(2) includes all stresses that are acting together in a given mode. The vector of the mode equivalent stresses reads (the indices $\sigma, \tau$ mark the fracture causing Mohr stress)

$$\left\{\sigma_{\mathrm{eq}}^{\mathrm{mode}}\right\} = \left(\sigma_{eq}^{||\sigma}, \sigma_{eq}^{||\tau}, \sigma_{eq}^{\perp\sigma}, \sigma_{eq}^{\perp\tau}, \sigma_{eq}^{||\perp}\right)^T. \tag{3}$$

Employing mode *strength* $\bar{R}^{\mathrm{mode}}$ and *equivalent stress* $\sigma_{eq}^{\mathrm{mode}}$, the following set of formulas for the stress effort of each of the 5 modes can be provided and its relationship to the associated equivalent stress: $F_{||}^{\sigma}$ (FF 1):

$$E_{ff}^{||\sigma} = \sigma_1 / \bar{R}_{||}^{t} = \sigma_{eq}^{||\sigma} / \bar{R}_{||}^{t} \text{ with } \sigma_1 \cong \varepsilon_1^t \cdot E_{||} \ (matrixnegligible), \tag{4a}$$

$F_{||}^{\tau}$ (FF 2):

$$E_{ff}^{||\tau} = -\sigma_1 / \bar{R}_{||}^{c} = +\sigma_{eq}^{||\tau} / \bar{R}_{||}^{c} \text{ with } \sigma_1 \cong \varepsilon_1^c \cdot E_{||}, \tag{4b}$$

$F_{\perp}^{\sigma}$ (IFF 1):

$$E_{ff}^{\perp\sigma} = [(\sigma_2 + \sigma_3) + \sqrt{(\sigma_2 - \sigma_3)^2 + 4\tau_{23}^2}]/2\bar{R}_{\perp}^{t} = \sigma_{eq}^{\perp\sigma} / \bar{R}_{\perp}^{t}, \tag{4c}$$

$F_{\perp}^{\tau}$ (IFF 2):

$$E_{ff}^{\perp\tau} = [(b_{\perp\perp} - 1) \cdot (\sigma_2 + \sigma_3) + b_{\perp\perp}^{\tau} \sqrt{(\sigma_2 - \sigma_3)^2 + 4\tau_{23}^2}]/\bar{R}_{\perp}^{c} = +\sigma_{eq}^{\perp\tau} / \bar{R}_{\perp}^{c}, \tag{4d}$$

$F_{\perp||}$ (IFF 3):

$$\begin{aligned} E_{ff}{}^{\perp||} &= \{[b_{\perp||}^{\cdot} I_{23-5} + (\sqrt{b_{\perp||}^2 \cdot I_{23-5}^2 + 4 \cdot \bar{R}_{\perp||}^2 \cdot (\tau_{31}^2 + \tau_{21}^2)^2}]/(2 \cdot \bar{R}_{\perp||}^3)\}^{0.5} \\ &= \sigma_{eq}^{\perp||} / \bar{R}_{\perp||} \end{aligned} \tag{4e}$$

with

$$I_{23-5} = 2\sigma_2 \cdot \tau_{21}^2 + 2\sigma_3 \cdot \tau_{31}^2 + 4\tau_{23}\tau_{31}\tau_{21}. \tag{5}$$

Above stresses include the nonlinearly load-dependent load stresses $\{\sigma\}_L$ and the equally nonlinearity dependent residual stresses $\{\sigma\}_R$ from curing etc.

An optimal use of the above failure conditions in numerical analysis is described in Cuntze (2010b).

### 2.5 Interaction of failure modes

What is only missing in chapter 2.4 is the interaction of failure modes. This is performed here by a probabilistic theory-based 'rounding-off' approach' formulated as a *series failure system* model

$$E_{ff}{}^{m} = (E_{ff}{}^{\text{mode 1}})^m + (E_{ff}{}^{\text{mode 2}})^m + ... + ... + ... = 1 \tag{6}$$

with the so-called (global) *stress effort* $E_{ff}$, representing the actual *portion of the 'load'-carrying capacity of the material,* and with a Weibull-related interaction coefficient m. The *mode stress efforts* $E_{ff}{}^{\text{mode}}$ are the contributions of each participating failure mode.

All three IFFs are interacted together with the FFs in one single 'global' failure equation

$$E_{ff}{}^{m} = (E_{ff\,||}^{\tau})^m + (E_{ff\,||}^{\sigma})^m + (E_{ff\,\perp}^{\sigma})^m + (E_{ff\,\perp||})^m + (E_{ff\,\perp}^{\tau})^m = 1. \tag{7}$$

For usually applied UD materials the value of m is between 2 and 3. From practical mapping experience approximately the same value may be taken for all interaction zones. Eq.(7) may be interpreted as an equation that considers the so-called *joint failure probability* of the failure modes. For more details the reader is referred to Cuntze (2004, 2010a,b).

For a 2D example, the interaction of the 3 IFF shall be visualized by Fig. 3. It depicts the straight pure mode curves and the interaction curve $(\sigma_2, \tau_{21})$. Herein, the stress efforts (FFs zero) of the 3 pure IFF modes (form straight lines in Fig. 3) read:

$$E_{ff\,\perp}^{\sigma} = \frac{\sigma_2}{\bar{R}_{\perp}^{t}}, \quad E_{ff\,\perp||} = \frac{|\tau_{21}|}{\bar{R}_{\perp||} - \mu_{\perp||}\cdot\sigma_2}. \quad E_{ff\,\perp}^{\tau} = \frac{-\sigma_2}{\bar{R}_{\perp}^{c}}, \tag{8}$$

wherein a simplified $E_{ff\,\perp||}$-formulation from Cuntze (2006) was used.

A general 2D mapping formulation reads $F(\sigma_1, \sigma_2, \tau_{21}, \bar{R}_{||}^{t}, \bar{R}_{||}^{c}, \bar{R}_{\perp}^{t}, \bar{R}_{\perp}^{c}, \bar{R}_{\perp||}) = 1$.

For UD fibre reinforced plastics the associated in-plane stresses-caused fracture is visualized in Fig. 4. The associate effort equation reads,

$$\left[\frac{\varepsilon_1^{t}\cdot E_{||}}{\bar{R}_{||}^{t}}\right]^m + \left[\frac{-\varepsilon_1^{c}\cdot E_{||}}{\bar{R}_{||}^{c}}\right] + \left(\frac{\sigma_2}{\bar{R}_{\perp}^{t}}\right)^m + \left(\frac{-\sigma_2}{\bar{R}_{\perp}^{c}}\right)^m + \left(\frac{|\tau_{21}|}{\bar{R}_{\perp||} - \mu_{\perp||}\cdot\sigma_2)}\right)^m = 1. \tag{9}$$

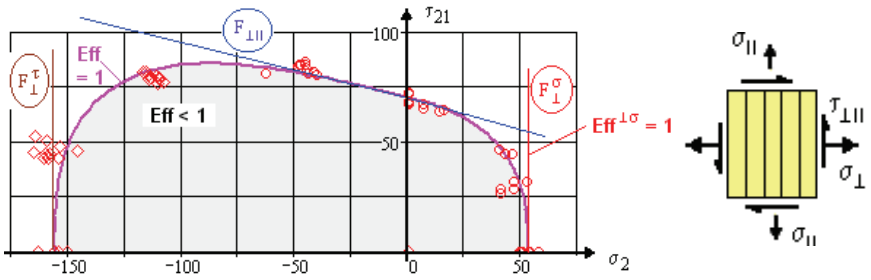


Figure 3: Visualization of the interaction procedure. Hoop wound GFRP tube, E-glass/ LY556/HT976.

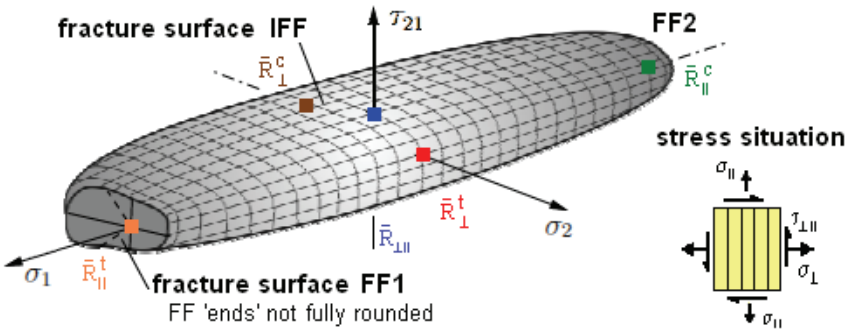


Figure 4: 2D failure surface of FRP UD lamina (courtesy W. Becker)

## 3 Specific Aspects in Validation

### *3.1 'Isolated' and 'embedded' properties*

Properties used as input for the analysis are generally test results from *isolated* UD lamina specimens such as a tensile coupon or a 90° wound tube. They are load-controlled achieved and are results of *weakest link* type behaviour whereas the in-situ behaviour of a (constraint) one-sided or two-sided UD lamina, *embedded* in a laminate, is deformation-controlled and therefore of *redundant type*, see Fig. 5. This fact shows up that a good mapping of the course of 'isolated UD test data' does not involve the full information necessary for a qualified analysis of laminates which consist of a stack of embedded laminas.

A non-linear analysis in the strain-softening domain of an embedded lamina has to consider both the positive effect from obtaining redundancy by the embedding and the adverse effect of notching neighbour layers by localizing of micro-cracks versus

the end of diffuse multi-site micro-cracking when approaching the so-called characteristic damage state (CDS). After reaching CDS, the number of micro-cracks practically remains about constant, whereas their width increases followed by forming of some larger discrete micro-cracks to macro-size, eventually followed by delamination. Above two facts form the in-situ effect.

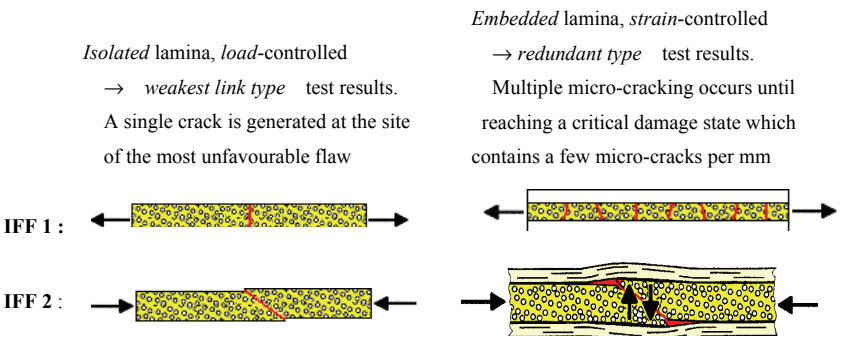


Figure 5: IFF features in isolated and embedded laminae (for $F_{\perp||}$ similar), [Puck, VDI97]

*In the context above one should keep in mind: 1) Each failure mechanism is affected by an associated typical state of stress. The failure mechanism with the highest stress effort will dominate the failure. A mode effort has to become zero if the mode driving stress is zero. 2) Due to IFF the curing stresses decay in parallel with the degradation. 3) The non design-driving stresses of a mode might increase or decrease the stress effort which is basically caused by the design driving stress. This influence is considered in the equivalent mode stress. 4)*$\sigma_2 \cong \sigma_3$ *activates the failure mode IFF1 in 'two planes' and thereby 'doubles' fracture danger. 5)*$\tau_{23}$ *activates two different failure modes, i.e. IFF1 and IFF2, according to the fact that the shear stress* $\tau_{23}$ *can be replaced by a normal tensile stress* $\sigma_2^t$ *with a compressive stress* $\sigma_2^c$ *with IFF1 being the critical mode for the brittle UD.*

Fig . 6 eventually shall depict the different criticality of the five UD failure modes.

### *3.2 Use of global and modal failure conditions*

There are two different formulations possible, a global formulation and a mode-wise (modal) formulation. The associated equations generally read:

One global failure condition (usual formulation) :

$$F(\{\sigma\},\{\bar{R}\}) = 1 \tag{10a}$$

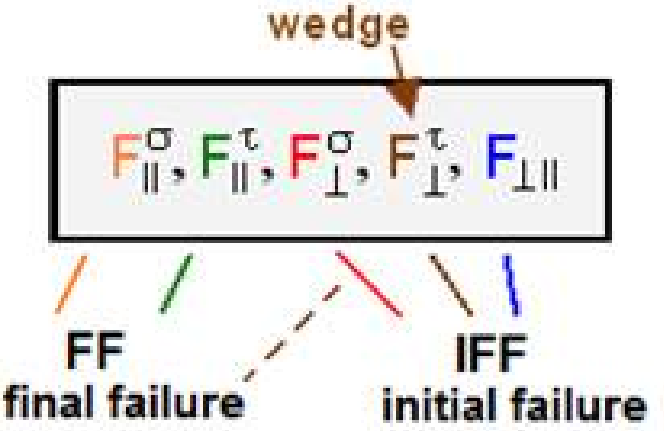


Figure 6: Failure mode criticality

Several mode failure conditions (FMC formulation) :

$$F(\{\sigma\},\{\bar{R}^{\text{mode}}\}) = 1. \tag{10b}$$

Most often, failure conditions map a course of multi-axial test data by one global equation not taking care whether the data belong to one or more failure mechanisms or failure modes. Therefore, extrapolations out of the mapping domain may lead to erroneous results. Further, if a correction change in the domain of one failure mode has to be made it may affect the failure surface or the curve domain of fully independent other failure modes. This is a mathematical consequence. Fig. 7 outlines the different curves achieved with the often used ZTL global failure condition and the FMC modal failure condition. As a visualizing example a case with a high scatter of the 'isolated' values is chosen. The arrows indicate that, when the transversal tensile strength $\bar{R}_{\perp}^{t}$ might have to be corrected after a new test series, the global curve will change in an independent but mathematically linked IFF domain. This is physically not correct. A FMC condition remains the same in an independent mode domain. In Eq.(11b) with the absolute signs numerically obtained senseless negative efforts are made zero. With the Föppl/Macauley brackets the same is achieved.

$$ZTL: \quad \frac{\sigma_2^2}{\bar{R}_{\perp}^{t}\cdot\bar{R}_{\perp}^{c}} + \sigma_2\cdot\left(\frac{1}{\bar{R}_{\perp}^{t}} - \frac{1}{\bar{R}_{\perp}^{c}}\right) + \frac{\tau_{21}^2}{\bar{R}_{\perp\parallel}^2} = 1 \tag{11a}$$

$$FMC: \quad \left(\frac{\sigma_2+|\sigma_2|}{2\cdot\bar{R}_{\perp}^{t}}\right)^m + \left(\frac{-\sigma_2+|\sigma_2|}{2\cdot\bar{R}_{\perp}^{c}}\right)^m + \left(\frac{|\tau_{21}|}{\bar{R}_{\perp\parallel}-\mu_{\perp\parallel}\cdot\sigma_2)}\right)^m = 1 \tag{11b}$$

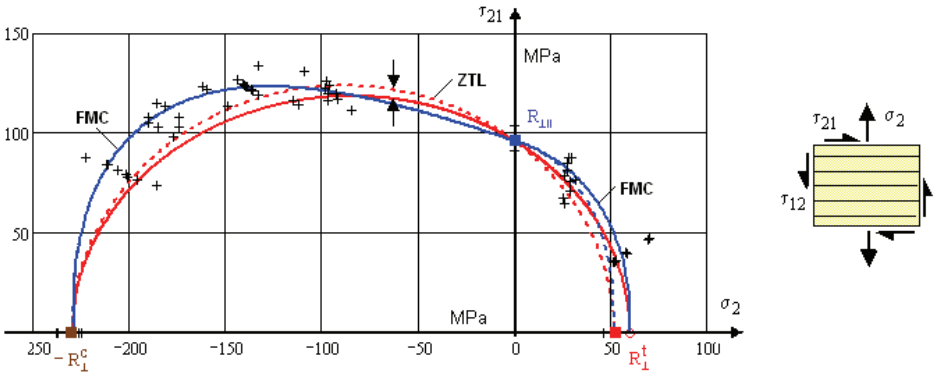


Figure 7: Consequences in use of global failure conditions. Hoop wound tube, T300/LY556/HY976; crosses mark test data

So, from application of global conditions the lesson was learned: A change, necessary in one failure mode domain, may have an impact on other physically not related failure mode domains, but in general not on the safe side.

### *3.3 Use of laminate fracture data*

Using fracture data from laminates should involve the consideration of 'embedded' lamina properties, see chapter 3.1. Therefore, the validation of UD lamina failure conditions becomes more difficult. However, after validation of the lamina failure conditions, laminate fracture data are used as benchmarks. The data help to understand the embedded (in-situ) effect in order to derive improvements for the input of the laminate analysis.

### *3.4 Healing effects in tri-axial compressive stress states*

Compressive stress states exhibit 'healing' (smoothing behaviour) effects due to redundancy. This can be recognized by some 'jumping' of the test data when bi- and tri-axial compression comes to act. Then torsion resistance increases not really continuously from $\sigma_2^c = 0$ on in negative direction.. Such effects occur with different intensity, i.e. test cases $(\sigma_2^c, \tau_{21})$ marginally, in $(\sigma_2^c, \sigma_3^c, \tau_{21})$ significantly.

### *3.5 Evaluation errors*

A correct analysis of boundary conditions and stress state of the test specimen is mandatory before evaluating and afterward applying the data in analysis. In this sense, tubes instead of the flat coupon specimens will help to avoid problems associated with the 'free edge effect'. Such a tubular specimen can be subjected to

internal and external pressure, to torsion and axial forces. A wide range of bi-axial stresses can be covered by them.

But, even tube testing is not free of problems such as barrelling (bulging), caused by end constraints, or buckling (is not a *strength* failure mode) of the cylinder. Further, tubes may exhibit non-linear changes in geometry during loading (widening). Therefore, a non-linear analysis has to take into account both, large strains *and* large deformations. If these facts are not considered in test evaluation *and* in analysis one has compared apples and oranges. Also in the WWFE data provision, in data evaluation un-deformed specimen geometry unfortunately has been used. This induced more or less essential errors and complicated validation.

Real tri-axial stress states require refined specimens (e.g. see Cuntze et al (1997); Fischer (2003)).

### *3.6 Residual stresses and thickness effect*

Residual stresses in a lamina of the laminate are decaying with decreasing stiffness caused by the degradation which accompanies increasing non-linearity. In other words: In parallel to the decay of the stiffness the non-linear analysis releases matrix-dominated stresses.

Thickness effect: Due to being strain-controlled, the material flaws in a *thin* lamina cannot grow freely up to micro-crack size in the thickness direction (this is sometimes called *thin layer effect*), because the neighbouring laminae act as micro-crack-stoppers. Considering fracture mechanics, the strain energy release rate responsible for the development of damage in the 90° plies from flaws into micro-cracks, increases with increasing ply thickness. Therefore, the actual absolute thickness of a lamina in a laminate is a driving parameter for initiation or onset of micro-cracks. A significant change of hoop stress may occur in a hoop-wound tube under hydrostatic pressure.

### *3.7 Depiction of failure stresses*

When trying to understand the experimental results one has to distinguish whether the test results are fracture values in total stresses or hydrostatic pressure superposed fracture stresses, Fig.8. This difference is not always clearly written in the given test information. From comparing data of various sources one can sometimes only sort out what might be meant. For the example UD lamina, tri-axial failure information can be provided in several ways ($\sigma_{hyd} = -p_{hyd}$):

$$\{\sigma\} = (\sigma_1, \sigma_2, \sigma_3, \tau_{23}, \tau_{31}, \tau_{21})^T$$

or

$$\{\sigma\} = (\sigma_1^{add} - p_1, \sigma_2^{add} - p_2, \sigma_3^{add} - p_3, \tau_{23}, \tau_{31}, \tau_{21})^T. \tag{12}$$

The stresses $\sigma^{add}$ are the 'external' stresses (also termed differential stresses) which may be increased up to $\sigma_{fr}^{add}$. This is the resistance value that marks the pressure-dependent multi-axial fracture state of stress. In order to correctly interpret the diagrams in the associated literature one has to carefully check whether the diagram is of the type $\sigma_{x,fr}(\sigma_y = \sigma_z, \bar{R})$ or of $\sigma_{x,fr}(p_{hyd}, \bar{R})$.

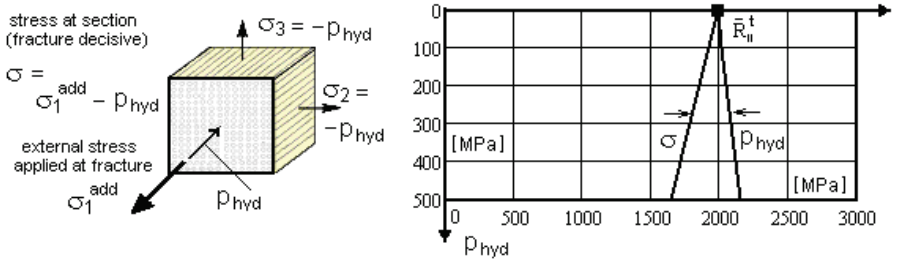


Figure 8: Different stresses in the multi-axial compression case

## 4 Validation of 2D Failure Conditions (WWFE-I)

### *4.1 Stress state $\{\sigma\} = (0, \sigma_2, 0, 0, 0, \tau_{21})^T$, TC1 in WWFE-I, PartB*

In the following it is referred to UD lamina test cases (TC) of the WWFE-I.

In Fig. 9 the circle-dotted curve shows the blind prediction in Part A on basis of the three provided strength values. The physically required friction value could not be provided. Therefore, a very low friction parameter (safe side) was used.

For Part B the friction parameter (average value for this physical quantity to be taken) could be assessed from curve data. All strength values had to be adapted due to new information in Part B. Then, the course of data could be mapped without any problems despite of the fact that the peak point is beyond of any other test result ever seen and measured, e.g. Fig. 3.. However it might be also possible that the strength value at the shear axis is too low and does not represent an average shear strength $\bar{R}_{\perp||}$. This idea is substantiated by own tests and another TC where the same material is used and where the shear strength corresponds to the Part A value. A 'normal' peak point would enable to map the scattering data at $\sigma_2^c \approx -115$MPa excellently.

*Lessons learnt: A prediction – in the frame of a validation – makes only sense if all physically necessary data are provided. The establishment of the Fig. 9 non-failure envelope requires 3 strengths plus a typical friction value.*

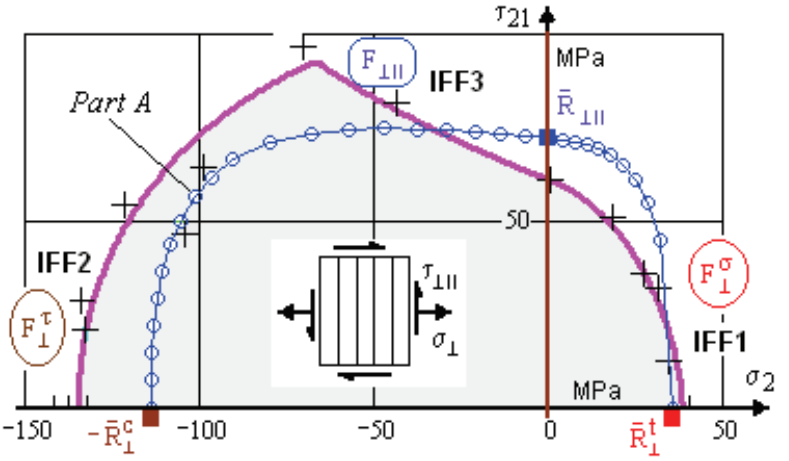


Figure 9: E-glass/LY556/epoxy

### *4.2 Stress state* $\{\sigma\} = (\sigma_1, \sigma_2, 0, 0, 0, 0)^T$

#### *4.2.1 Case* $\{\sigma\} = (\sigma_1^t, \sigma_2^c, 0, 0, 0, 0)^T$*, TC6 in WWFE-I*

The solid curve in Fig. 10 shows the prediction on basis of the provided strength data. For this test cases, knowledge about the friction parameter was not required in this TC.

For Part B the strength values could be kept. The delivered test data show a gap in the fourth quadrant of Fig. 10. Such a gap belongs to a non-regularity in testing. Therefore, no attempt is made to better map the course of data.

*Lesson learnt: Performing reliable experiments is a very challenging task.*

#### *4.2.2 Case* $\{\sigma\} = (\sigma_1^c, \sigma_2^c, 0, 0, 0, 0)^T$

In the WWFE-I no test data in quadrant III could be provided. With a special test equipment IKV-Aachen, Fischer (2003), tried to fill this gap, and to prove that an interaction exists between FF2 (kinking failure) and IFF2 (wedge failure). As test method, a 4-point-bending method applied to a 2-layer laminate composed of an upper T300 'face sheet' as critical layer and a 'supporting' T700/epoxy layer which is stronger than the T300/epoxy.

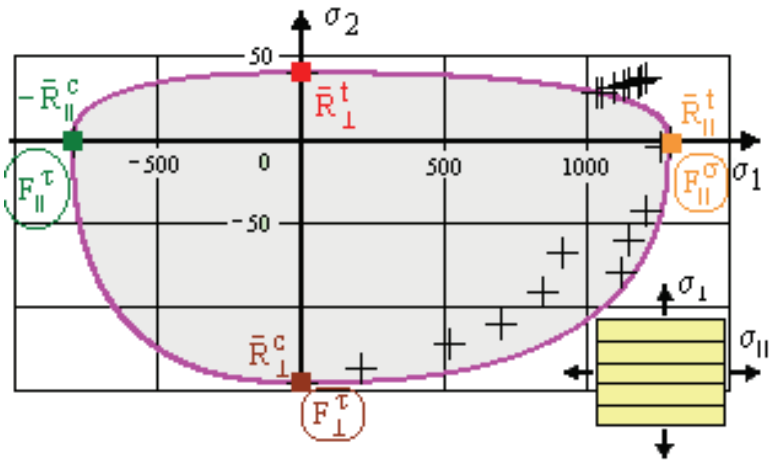


Figure 10: Bi-axial non-failure stress envelope $(\sigma_2^c, \sigma_1^t)$. UD-lamina. E-glass/MY750epoxy. Hoop wound tube data, $m = 3.1$. $\sigma_1 \equiv \sigma_{hoop}$, $\sigma_2 \equiv \sigma_{axial}$ Provided: $\{\bar{R}\} = (1280, 800, 40, 145, 73)^T$

In Fig. 11, the obtained test results are depicted by crosses. They indicate a too high FF2 resistance (kinking mode). This fact can be physically explained: The test layer is one-sided embedded and not fully isolated any more. Some sort of an elastic foundation effect takes place and increases kinking resistance.

*Lesson learnt: Proof of the presumption is achieved. It can be concluded that with increasing $\sigma_2^c$ the resistance in fibre direction is reduced (The term strength should be restricted to the measured 5 (basic) strengths). A chance for executing an 'isolated' test seems to be not given.*

As a warning, the Tsai-Wu curve is included in the diagram in order to show the shortcoming of the Tsai-Wu failure conditions in this quadrant.

*Lesson learnt: Tsai-Wu is not applicable here, even after using a Tsai parameter of $\tilde{F}_{12} = -0.4$.*

### *4.3 Stress states* $\{\sigma\} = (0, \sigma_2, 0, 0, 0, \tau_{21})^T$, $\{\sigma\} = (0, \sigma_2, 0, 0, \tau_{31}, 0)^T$

Fig. 12 displays the difference between the two in-plane shear curves. The shear resistance is not increased in the negative $\tau_{31}(\sigma_2)$domain. The same applies for $\tau_{21}(\sigma_3)$.

*Lesson learnt: The shear $\tau_{31}$ does not act together with $\sigma_2$. This has to be considered by the IFF3 failure condition. The shear stresses $\tau_{21}, \tau_{31}$ are the fracture causing stresses, not the associated shear stresses $\tau_{12}, \tau_{13}$.*

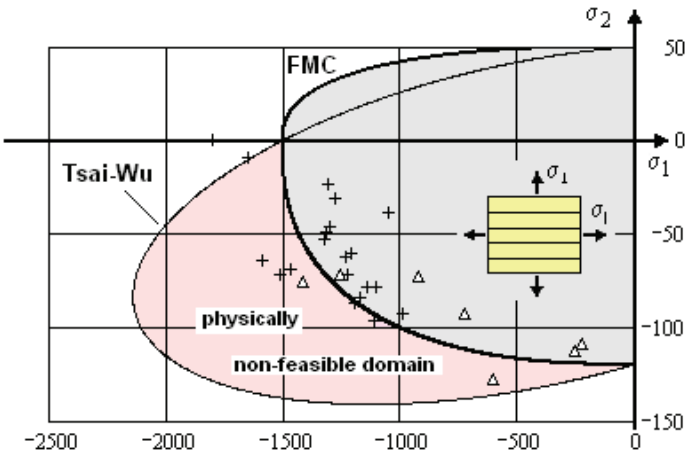


Figure 11: Bi-axial fail. stress envelope $(\sigma_2^c, \sigma_1^c)$ in MPa. UD-lamina. T300/LY556/HY917/DY070. Tsai-Wu:$\tilde{F}_{12} = -0.4$

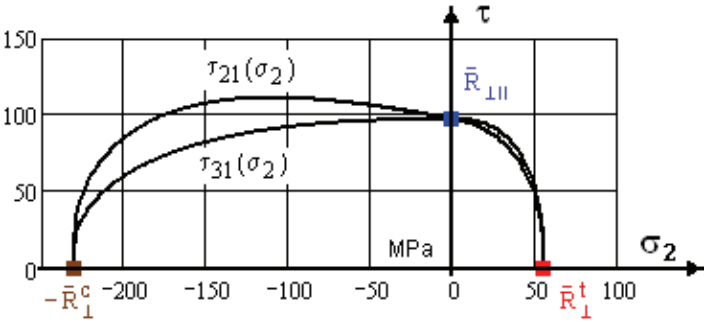


Figure 12: Difference of shear fracture curves

### *4.4 Stress state $\{\sigma\} = (\sigma_1, 0, 0, 0, 0, \tau_{21})^T$, TC2 in WWFE-I Part B*

Attention has to be paid to not mixing up test results which are apples and oranges. The situation in Fig. 13 shows a bi-axial non-failure stress envelope $(\tau_{21}, \sigma_1)$. he loading is torsion with internal pressure plus axial loading. The crosses belong to failure data from 90°-wound tube test specimens and the others to axially wound 0° tube specimens. The 0° tube test data exhibit a too large scatter and 'jumping' in the positive domain, which disqualifies the 0° data.

However, there is a possibility to use the 0° test data together with the 90° test data. The axially wound tube is heavily shearing under torsion loading. Conse-

quently, the data given are not the searched lamina stresses $(\tau_{\perp||}, \sigma_{||})$ but stresses belonging to the structure coordinate system (x,y). Therefore, an attempt is made to re-evaluate the experimental data in two steps: At first, one determines an estimate of the (non-provided) shear angle $\gamma$ by a non-linear CLT analysis and secondly, one transforms the stress data provided into the real (||-⊥) coordinate system of the lamina. The computation will deliver the real lamina stresses, as follows:

$$\begin{aligned}
\sigma_{||} &= \sigma_x(\cos\gamma)^2 + 2\tau_{yx}\cos\gamma\sin\gamma, \\
\sigma_{\perp} &= \sigma_x(\sin\gamma)^2 - 2\tau_{yx}\cos\gamma\sin\gamma, \\
\tau_{\perp||} &= -0.5\sigma_x\sin 2\gamma + \tau_{yx}\cos 2\gamma.
\end{aligned} \tag{13}$$

For instance for the point $(\sigma_x, \sigma_y, \tau_{yx})$= *(1000, 0, 123),* $\gamma$=*+3*° was obtained and after transformation the lamina stress state $\Rightarrow (\sigma_{||}, \sigma_{\perp}, \tau_{\perp||})$ = (1010,-10, 70) MPa. The angles 3° and –2° in Fig. 13 result in size (rounded) and sign from the above described CLT computation that uses the corresponding set of combined fracture stresses given. The finding for the two chosen 0° test points is: Both corrected test points practically fall (by chance fully) on the existing mapped curve. The discrepancy is vanished!

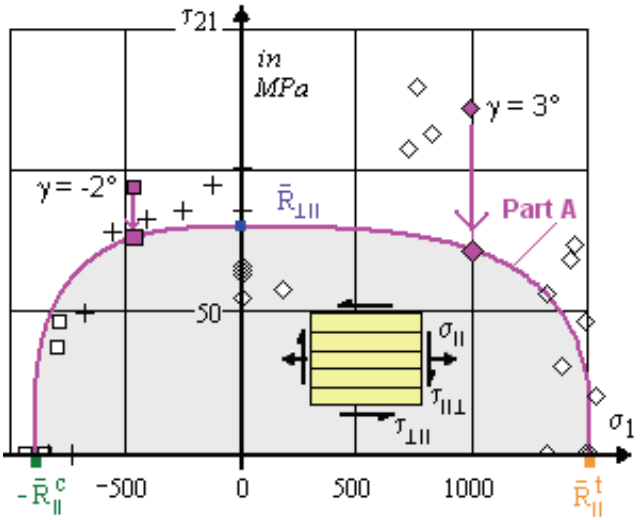


Figure 13: Difference of fracture shear stress results from hoop and axially wound tubes. Bi-axial non-failure stress envelope. UD-lamina T300/BSL914C epoxy, $\{\bar{R}\} = (1500, 900, 27, 200, 80)^T$. $m = 3.1$.

*Lesson learnt: For 0° test data the axes cannot be termed* $\tau_{21}$ *and* $\sigma_1$.

### *4.5* ***Stress state*** $\{\sigma\} = (0, \sigma_2, \sigma_3, 0, 0, 0)^T \equiv \{\sigma\} = (0, \sigma_2, \sigma_3, \tau_{23}, 0, 0)^T$

Fig. 14 represents a *non*-failure envelope for a bi-axial normal stress state. The bi-axial strength $R^t_{\perp\perp}$ shall indicate that in this corner a twofold danger to fracture exists. For high bi-axial compression states – due to the Poisson effect - the IFF1/IFF2 envelope is closed by FF1.

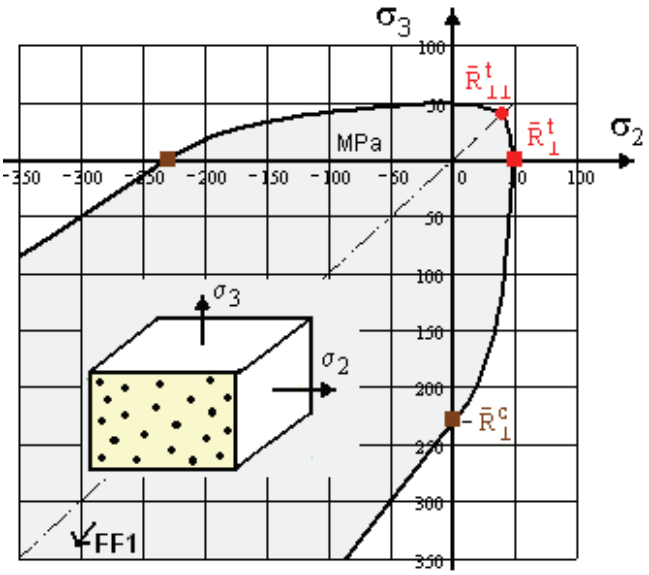


Figure 14: Fracture curves in case of bi-axial normal stresses. $b_{\perp\perp} = 1.2$

*Lesson learnt: Reliable UD test data ($\sigma_2^c, \sigma_3^c$) are not available, presently. However, cast iron behaves similarly in this quasi-isotropic plane and its data may be used as supporting information, see Cuntze (2008).*

## 5 Validation with UD lamina-composed Laminate Data, WWFE-I

Most engineers assume that FF in at least one lamina of a laminate means final failure of the laminate. Therefore, the bi-axial non-failure envelopes for final failure of laminates predicted by the various authors do not differ that much, as long as the laminates are 'well-designed and have three or more fibre directions. The multi-axial 'strength', better resistance, of these laminates is 'fibre dominated'. Further, the predicted stress-strain curves of such laminates look very similar because the fibres being much stiffer than the matrix carry almost the full loads. Different degradation procedures after the onset of inter-fibre failure (IFF) do therefore not

influence the predicted strains very much. This is especially true for CFRP laminates.

### 5.1 Laminate stress-strain curve $\hat{\sigma}_y(\hat{\varepsilon}_x)$, $\hat{\sigma}_y(\hat{\varepsilon}_y)$ under bi-axial loading (angle-ply), TC11

This TC of the WWFE-I, Fig. 15, needs a special carefulness, because prediction and experiment show big a discrepancy. The test specimen is a balanced angle-ply tube (water hose).

The roof sign shall indicate that the stress is an average (smeared) stress of the laminate.

For the assessment of the test data curve in Puck and Schuermann (2002) the following two CLT-based equationswhich means for a tube under internal pressure with the ideal $\pm\arctan\sqrt{2}$ fibre orientation 54.75°,

$$\hat{\varepsilon}_x = \varepsilon_1 - \gamma_{21}/\sqrt{2}, \quad \hat{\varepsilon}_y = \varepsilon_1 + \gamma_{21}/(2\cdot\sqrt{2}) \tag{14}$$

are cited. They confirm that the two stress-strain curves should be finally parallel, because the shear strain will not change its sign. This is substantiated because in the case of the full validity of net theory both curves would be identical, but of course net theory can only deliver the tendency.

The author himself sorted out from the Part B provided data that the tensile failure strain was higher than the value that belongs to the physical fracture loading. A shift versus the triangle in Fig. 15 might be seen probably, however, the test curve is lower and by that leaves another discrepancy.

Eventually the IKV Fischer (2003); Knops (2003) performed special tests using tubes wound from GFRP and CFRP. Results, when subjected to internal pressure loading showed an extreme dependency on small variations of the orientation angle. In parallel, this finding was analytically investigated (non-linear with a degradation function in strain-softening for $E_\perp$, $G_{||\perp}$, but not for the in-plane Poisson's ratio $\nu_{\perp||}$ (larger ratio). These results confirm the sensitivity and prove that angle deviations drift under degradation towards the ideal net theory angle 54.75°. With increasing winding angle the critical $\sigma^t_\perp$ is reached at a somewhat lower pressure loading level and also IFF1. A further finding was that a CFRP tube with its higher anisotropy-ratio $E_{||}/E_\perp$ is more significantly affected than a GFRP; the stiffness change of the virgin CFRP is higher for the same angle deviation.

*Lesson learnt: The provided angle is not accurate enough to serve as validation basis. A crossing of the curves cannot be realistic. The data background has to be examined.*

### 5.2 *Laminate stress-strain curve $\hat{\sigma}_y(\hat{\varepsilon}_x)$, $\hat{\sigma}_y(\hat{\varepsilon}_y)$ under uni-axial loading (angle-ply), TC10*

In Fig. 16 the same tubes are used as before, just the loading is now radial. This loading causes a hoop stress $\hat{\sigma}_y$ in the laminate. The figure depicts two stress-strain curves of the simple laminate above but now under radial loading. The prediction has two shortcomings: stiffness is higher from the origin on when compared to the slope found in experiment, and the measured higher strains could be not calculated by the author's handmade tool **?** using Mathcad. For Part B, a modulus decrease could have introduced to better map the data curve. The sensitivity of deviations of the given fibre angle plays a role, too.

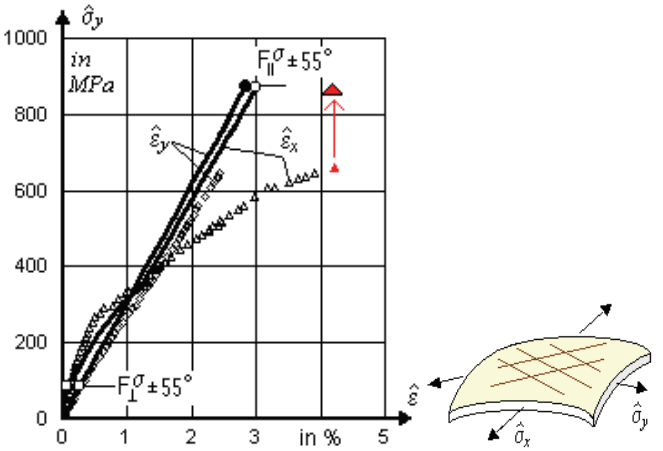


Figure 15: Stress-strain curves for $\hat{\sigma}_y : \hat{\sigma}_x = 2:1 (p_{int})$, [+55/-55/55/-55]-laminate. E-glass/ MY750 . ΔT= -68˚C. $\hat{\sigma}_y = \hat{\sigma}_{hoop}$. Final blind prediction point .

*Lesson learnt: The quality of theory and non-linear coding in managing the load transfer from matrix to the fibres determines the quality of the analytical results. However, as practice requires well-designed (w.r.t. loading) laminates their analysis becomes not that non-linear in real life. For lightweight structures the design strain is usually smaller than 0.6%.*

### 5.3 *Laminate stress-strain curve $\hat{\sigma}_y(\hat{\varepsilon}_x)$, $\hat{\sigma}_y(\hat{\varepsilon}_y)$ under multi-axial loading (cross-ply), TC13*

Fig. 17 shall outline some typical errors one can generate when evaluating test results without the high carefulness needed. The test specimen is a balanced cross-ply laminate tube whereas Fig. 16 addressed an angle-ply tube.

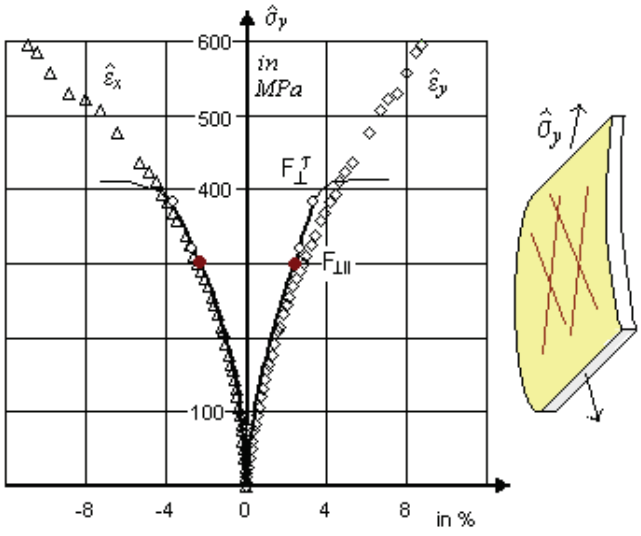


Figure 16: Stress-strain curves for $\hat{\sigma}_y$ : $\hat{\sigma}_x$=1:0 (radial loading by $p_{int}$ + axial compression load). Tube. [+55/-55/55/-55] -laminate, E-glass/MY750; ΔT= -68˚C. $\{\bar{R}\} = (1280, 800, 40, 145, 73)^T$ y:=hoop direction.$\hat{\sigma}_y \equiv \hat{\sigma}_{hoop}$. Final blind prediction point

Both the test curves of the cross-ply should approximately lie on top of another the symmetric geometry and due to loading. Different curves for $\hat{\varepsilon}_x$ and $\hat{\varepsilon}_y$ might indicate some bulging, however.

Hence one should check the evaluation of the test results: At fracture -according to micro-crack spacing- net theory can be applied to roughly assess test data values of this well-designed laminate.

In order to better understand the test curves a simple analysis shall be performed. From Part B, as input for the simple computation can be taken: $\varepsilon_x^{fracture} = 2.18\%$, $\varepsilon_y^{fracture} = 2.48\%$, and $\sigma_{\perp} = \tau_{\perp||} = 0$ due to the zero matrix stiffness assumed in the net theory model. With these values the net theory model *at first* lets conclude that for this fibre-dominated laminate the maximum *experimental* strength of *430MPa could be increased* (vertical arrow) up to $\hat{\sigma}_x = \hat{\sigma}_y$= *530MPa. Secondly,* a lower effective tensile strength $\sigma_{||}^{t}$=*1062MPa* is derived. And from this, the maximum *theoretical* fracture stress of 660*MPa*, according to the effective fracture strength values, may be *reduced* down to a value of $\hat{\sigma}_y = 660 \cdot 1062/1280 = 547 MPa$ which is to be correlated with the provided fibre tensile strength of *1280MPa*. As bulging was reported in experiment and proven by $\hat{\varepsilon}_y > \hat{\varepsilon}_x$. This results in a loop stain and

a hoop stress which are higher than the vessel formula used in test data evaluation delivered as provided data Twofold $F_{||}^{\sigma}$failure in both 45˚ layers will reduce the theoretical fracture value a little more.

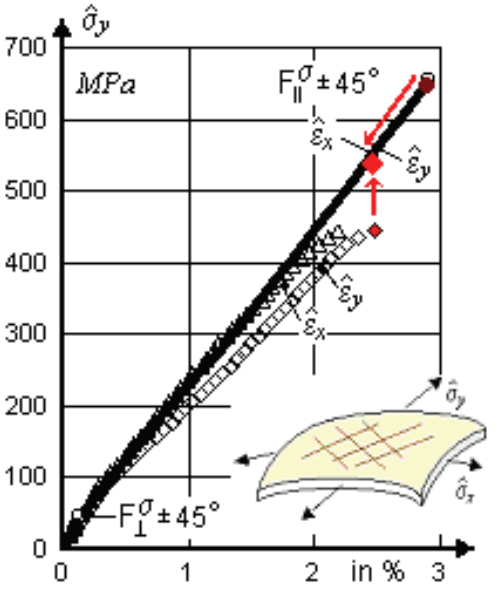


Figure 17: Stress-strain curves for $\hat{\sigma}_y : \hat{\sigma}_x = 1:1, (p_{int}+\cdot$ axial tension). [+45/-45/45/-45]-cross-ply laminate. E-glass/MY750. ΔT= -68˚C. Final blind prediction point. Maximum test value after correction.

*Lesson learnt: Bulging seems to be responsible that the test curves do not lie on another and for a real fracture stress higher than the 440 MPa. Part B information seems not to be fully consistent.*

### *5.4 Laminate initial and final non-failure envelope $\hat{\sigma}_y(\hat{\sigma}_x)$, TC4*

Fig. 18 concerns a tube subjected to pressure loading combined with axial loading. The formulas for the test evaluation are

$$\hat{\sigma}_{hoop} = p(r_{int} + \Delta r)/t, \quad \hat{\sigma}_{ax} = pr_{int}/2t + F/(2\pi \cdot r_{int} t)$$

with laminate thickness $t$, applied force $F$, and the interior radius $r_{int}$.

Deficiencies are essentially located in quadrant III. The too few tests carried out under external pressure and axial compression can be not mapped by a *material*

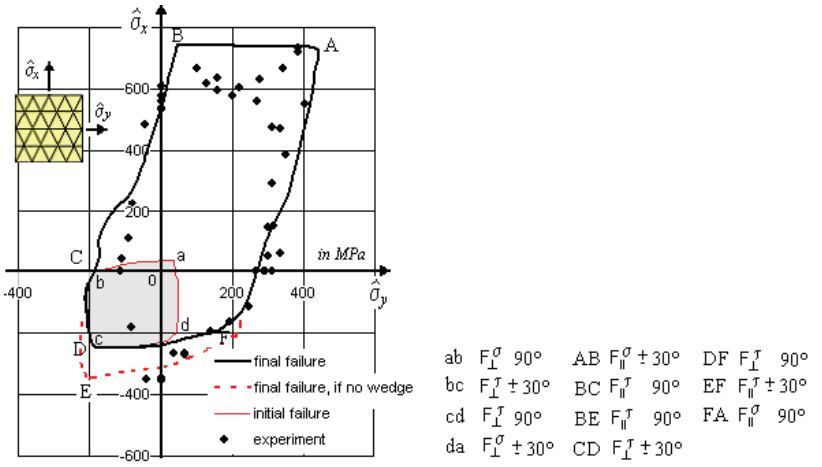


Figure 18: Initial and final biaxial non-failure envelope $\hat{\sigma}_y\,(\hat{\sigma}_x)$. [90/30/-30/30/-30/90]$_n$-laminate. Hoop wound tube, liner. E-glass/LY556epoxy. $b_{\perp\perp} = 1.5$, $b_{\perp||} = 0.13$, $m = 3.1$.$\{\bar{R}\} = (1140, 570, 35, 114, 72)^T$.

failure condition, as they are governed by buckling (*structural* failure condition needed). A non-linear buckling analysis which considers the real imperfection geometry would help to sort out essential effects.

In quadrant IV kinking failure FF2 takes place. An increase of the Part A provided relatively low $\bar{R}_\perp^c = 114$ to 138 MPa allows mapping. This is depicted by the dashed curve.

The achieved maximum load on the negative hoop axis ($\hat{\sigma}_y$) is about 50% lower than that on the negative $\hat{\sigma}_x$-axis, because the pure x-loading of the cylinder is less buckling-critical according to the higher stiffness in axial direction than external pressure combined with axial tension load (failure caused by IFF2, $F_\perp^\tau 90°$). A further explanation for the discrepancies: The external 90° layer ($\hat{\sigma}_y^c$, p, F) becomes stabilized by biaxial lateral compression ($\sigma_2^c, \sigma_3^c = -p_{ext}$), and the filaments of the internal 90° layer are a little stabilized by the curvature of the shell. (2) An increase of $\bar{R}_{||}^c$ would help to fit the test data on the $\hat{\sigma}_x^c$-axis. The author believes that coupon buckling led to the low value of $\bar{R}_{||}^c = 570MPa$.

Mind: sharp corners of a failure curve would be rounded by regarding the joint failure probability.

*Lesson learnt: Maximum points such as point A show what might be reached. Lower values confirm stochastic scatter but also represent probable test short comings. Structural failure points (buckling) are not usable for a validation of material*

*failure conditions.*

With the next test cases the 3D capacity of the derived UD failure conditions shall be checked.

## 6 Validation of 3D Failure Conditions by lamina data (WWFE-II)

### *6.1 Stress state* $\{\sigma\} = (\sigma_1 = \sigma_3, \sigma_2, \sigma_3, 0, 0, 0)^T$*, TC5 of WWFE-II*

In this TC, rectangular blocks, cut from filament wound UD panels, were examined under combined axial loading with lateral pressure. During test, a hydrostatic pressure was first increased to a pre-determined level and then kept constant while the transverse compressive stress $\sigma_2^c$ was increased continuously until the specimen fractured. Task is the prediction of the non-failure envelope in all four quadrants. However for validation, test data are provided for the lower branch in quadrant III, only. Therefore, a comparison can be only made in quadrant III which means in the tri-axial compression domain. In the provision of data some problems with understanding of the given stresses arose (see chapter 3.1) and were solved by the organizer.

The slope of the course of Part B test data showed that the UD material is less brittle than assumed in Part A (curve not shown here). In consequence, the friction parameter $b_{\perp\perp}^{=}$ 1.21, chosen in Part A, was lowered to 1.14 and secondly as lateral strength the average value of the provided 3 test data is taken. This means the Part A value $\bar{R}_{\perp}^{c} = 145 MPa$ is to be replaced by 132 *MPa.*

*Lessons learnt: After re-evaluation of the failure stresses by Qinetic the above course of Part B data was provided. Mapping caused then no problem due to the fact that* $b_{\perp\perp}$ *and* $\bar{R}_{\perp}^{c}$ *had to be adapted to the provided Part B data.*

### *6.2 Stress state* $\{\sigma\} = (\sigma_1,\ \sigma_2, \sigma_3, 0, 0, \tau_{21})^T$*, TC2*

The test specimen is a filament wound tube. During test, the hydrostatic pressure was first increased to a pre-determined level and then kept constant while the in-plane fracture shear stress $\sigma_2^c$ was increased continuously until the specimen fractured. Problem was the influence of hydrostatic pressure $p_{hyd}$ on IFF3, or the fracture failure curve $\tau_{21,fr}(p_{hyd})$ with $\sigma_1 = \sigma_2 = \sigma_3 = -p_{hyd}$, and $p_{hyd}$ an absolute pressure value, Fig. 20.

The course of the scattering test data could be well mapped after an interpretation of the the sudden increase (jump) at zero hydrostatic pressure. This is assumed to be the consequence of the healing $p_{hyd}$ and was modelled in an adequate, simple way. Check point for TC2 and the two other linked test cases TC3 and TC4 is the open square. TC2 and TC 3 are not treated in this paper.

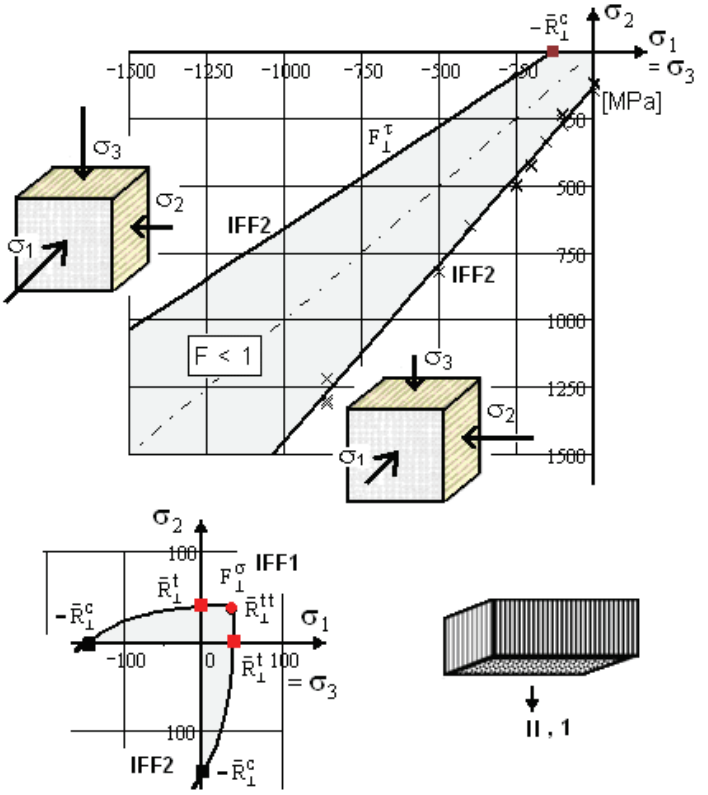


Figure 19: Tri-axial failure state of stress $\sigma_2(\sigma_1 = \sigma_3)$ for a UD E-glass/MY750epoxy. $\sigma_1$ is the stress acting at the respective coupon surface; the diagonal is the $p_{hyd}$ -line. $\{\bar{R}\} = (1280, 800, 40, 132, 73)^T MPa, \nu_{\perp||} = 0.28$, m = 2.8, $b_{\perp\perp} = 1.14$

*Lesson learnt: The $\sigma_2^c$ domain shows some healing redundancy and has, therefore, to be mapped for itself. Thereby, as model shear fracture strength 107 MPa is used. Early after a common interpretation of the information on the three linked test cases TC2 through TC4 a common check point in all 3 figures of Cuntze (2010b) could be found.*

### *6.3 Stress state $\{\sigma\} = (\sigma_1, \sigma_2, \sigma_3 = \sigma_2, 0, 0, 0)^T$, TC7*

In Fig. 20 data from tests executed with dog-bone test specimens are displayed. Searched is the longitudinal fracture stress $\sigma_{1,fr}(\sigma_2 = \sigma_3)$. Failure modes observed are longitudinal splitting, kinking, kink band.

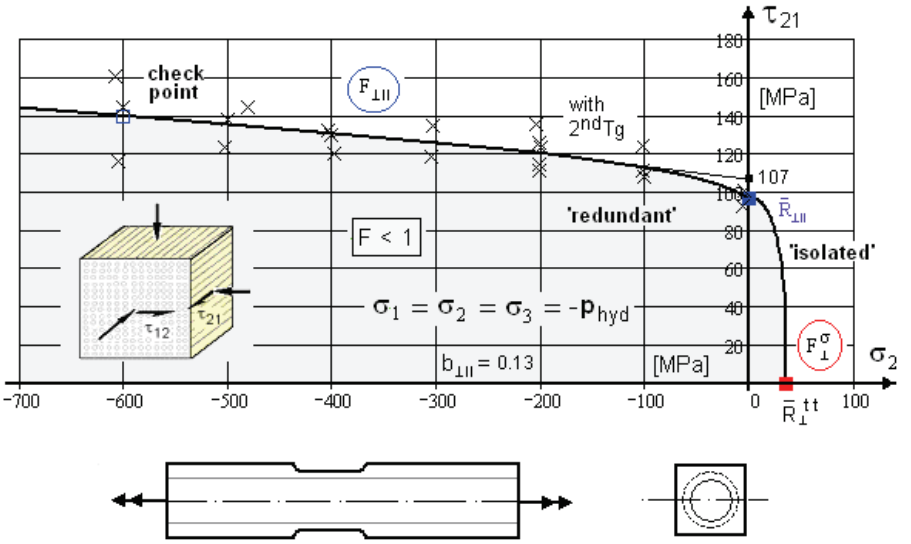


Figure 20: Fracture stress $\tau_{21,fr}$ vs stress $\sigma_2 (= \sigma_1 = \sigma_3 = -p_{hyd})$ for a UD T300 carbon/ PR319 epoxy. $\{\bar{R}\} = (1378, 950, 40, 125, 97)^T$ MPa. $\nu_{\perp||} = 0.32$. m = 2.8, $b_{\perp||} = 0.13, \nu_{23} = 0.5$.

Some discrepancies disturb the use of the provided test data for model validation. It is not understood why the tendency of the curves in quadrant III and IV is so different. Primarily, Poisson's effect is acting at bi-axial states of compression. This effect always causes tensile straining in the filament. Therefore, the compressive failure strain and similar the failure stress (acting at the cross section) is increased in quadrant III, whereas in quadrant IV the tensile failure strain (right curve) is reduced. This would result in a similar curvature tendency.

Part B test data show a non-consistent tendency, however. With increasing fracture failure strain the compression curve becomes more horizontally and the tension curve more vertically. How long the vertical drop will go (the provided data set ends at $\sigma_2 = \sigma_3 = -300MPa$) is not demonstrated. In another literature it is proven that the tensile fracture stress will reduce with $p_{hyd}$ till $-860MPa$ and this is in the sense of the Poisson effect.

In quadrant IV, it looks at $-150MPa$ either as if the fracture strain is reduced or as if the Poisson effect would have doubled. Below the bi-axial compression level of $\sigma_2 = \sigma_3 = -300MPa$, the Poisson effect 'vanishes' and the tensile stress - acting at the cross-section - keeps the same value of about $1500MPa$. In other words, the fracture strain of the filament would increase. Usually, the matrix reduces stiffness

and this would increase the Poisson effect and cause the opposite curvature or tendency of the provided data curve. It would become flatter instead of steeper or - as here – practically vertical. Even if the interphase material between filament and matrix will break then the bi-axial pressure would cause a reaction of the filament linked to its Poisson's ratio $\nu_f$ which is not so much different to the UD value $\nu_{12}$ .

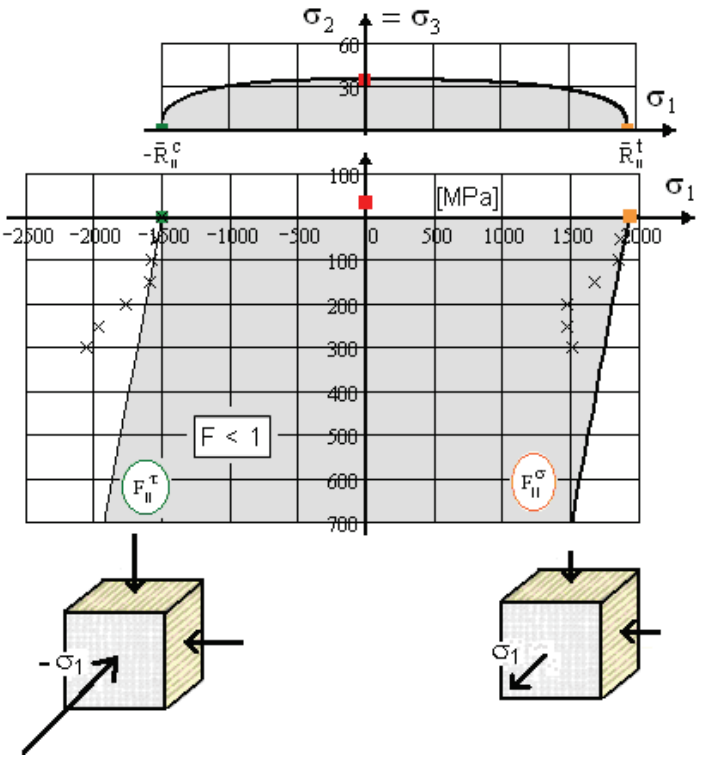


Figure 21: Through-thickness stress $\sigma_3 (= \sigma_2)$ vs. fibre-parallel stress $\sigma_1$. UD A-S carbon/epoxy1. $\{\bar{R}\} = (1990, 1500, 38, 150, 70)^T MPa, \nu_{\perp||} = 0.3$. m = 2, $\{\varepsilon_{fr}\} = (2.81, 1.75, 0.25, 1.2, 4)^T \%$. Data from fit of provided stress-strain curves: $\{\bar{R}_{p0.2}\} = (-, -, 156, 137, 54.6)^T$ MPa.

*Lessons learnt: Even after re-evaluation of the failure stresses by Qinetic the discrepancies did not vanish and the author is still not able to explain the discrepancies. The tendency in quadrant IV is not understood. Influence on the curve have: The in-plane Poisson's ratio $\nu_{12}$ (the smaller $\nu_{12}$, the steeper the curve), the 'healing' effect from bi-axial compression (may increase failure strain), and the so-called $2^{nd}$Tg effect of the matrix beyond $p_{hyd} > 200MPa$, tackled in Cuntze (2010b). Was measurement and test data evaluation correctly executed?*

## 7 Validation of 3D Failure Conditions by Laminate Data (WWFE-II)

### *7.1 Stress state* $\{\hat{\sigma}\} = (0_{,0}, \sigma_z, \hat{\tau}_{zy}, 0, 0)^T$*, TC10 in WWFE-II*

Searched is the *through-thickness failure shear stress* $\tau_{yz,fr}(\hat{\sigma}_z)$.In Part A, an Arcan test rig has been assumed by the author. This led to a fully different failure curve for the laminate specimen.

Fig. 22 shows test specimen and test rig as used for obtaining the Part B test data. Test specimens were tubes, machined from thick panels into small 'dog-bone pieces' having a hollow cylinder gauge section and square ends for applying torque. The specimens were subjected to combined axial compression and shear (torque). A constant axial compression load was applied first and then the specimen was twisted to failure under torque control. The fracture stress obtained when squeezing this quasi-isotropic laminate is expected to be higher than $\hat{R}_3^{squeezing} = 780MPa$.

Before including the provided approximate squeezing fracture value of the (structure) laminate into the (material) strength failure condition it should be clarified that the type of fracture is to some extent of a material failure mode nature. For instance, if filaments of the stacked layers come to lie upon another, this leads to a failure which is not covered by a material strength failure condition. In this context, one has to check whether the added quasi-isotropic laminate fracture values $\sigma_{z,fr}$ will really represent a final material failure. Nevertheless it is clear that onset of squeezing practure of a laminate (not micro-cracking etc. anymore) is the "end" of further operational use.

As the specimen is milled from a laminate brick edge effects (singularities) occur and stress concentrations as well. Further, a non-smooth shear stress field at the cross-section plane is present. Therefore, it can be stated that the test specimen does not give clear experimental evidence. The specimen encounters multi-site failure within each lamina and at the same time in all laminas (multi-ply failure). This means that a multi-fold fracture danger is given in the stack which also lowers the failure curve. It can be concluded that this specimen is not an adequate tool to validate a strength failure condition.

The test specimen could not be traditionally modelled, analytically or by FEA. A simple linear strength model was applied at the critical location which considers the inter-acting inter-laminar stress state ($\sigma_3, \tau_{31}, \tau_{23}$).

*Lessons learnt: If one does not know test specimen and test rig one cannot make a prediction. The specimen is not an adequate tool for validation. Despite of the fact that mapping could be achieved the results cannot be generalized for design purposes.*

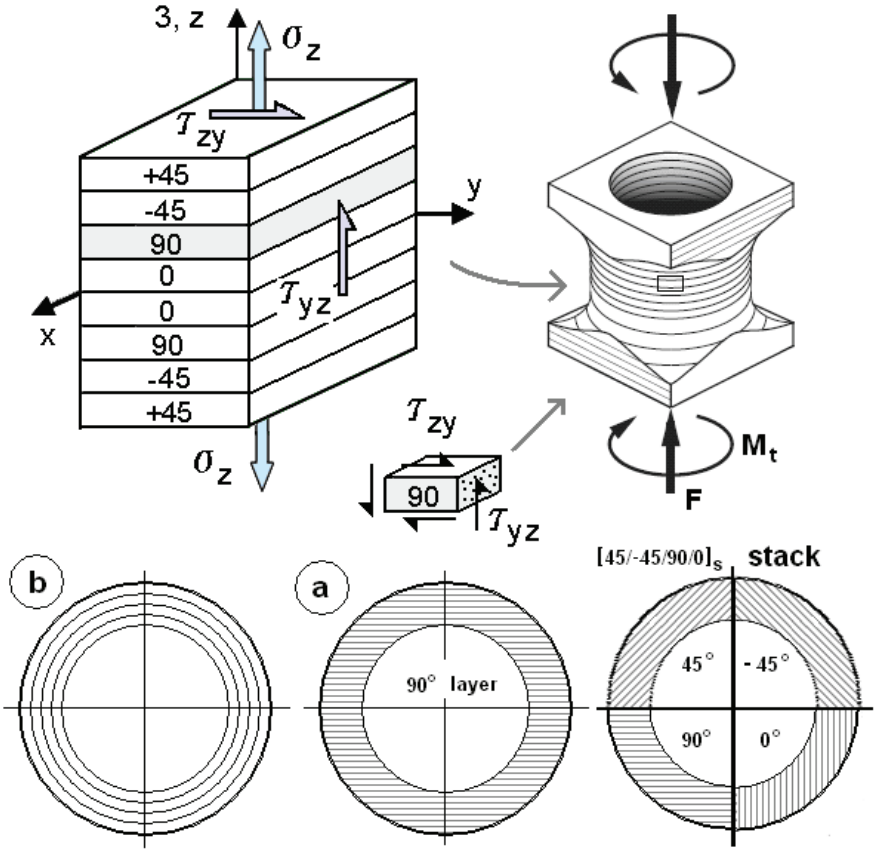


Figure 22: Applied section shear load-caused maximum-thickness failure shear stress $\tau_{zy}$ vs. applied through-thickness stress $\sigma_z$ for a [45/-45/90/0]$_{ns}$, carbon/epoxy laminate, IM7/8551-7. Figure a shows a 90˚-lamina of the stack of the tube milled from a laminate block (for comparison figure b shows the traditional wound or tape-layered tube); $b_{\perp\perp} = 1.21, b_{\perp||} = 0.3. t_k = 0.25mm$. $\{\bar{R}\} = (2560, 1590, 70, 185, 90)^T MPa$, $R_3^{squeezing} = 780MPa$. $\nu_{\perp||} = 0.34, m = 2.8$.

### *7.2 Stress state* $\{\hat{\sigma}\} = (0,0,\sigma_z,0,0,0)^T$*, TC12 in WWFE-II*

The test specimen is a balanced cross-ply laminate block that is compressed in thickness direction by a surface pressure $\sigma_z = -p$. To be predicted are the (average) strain-stress curves of the in-plane normal strains $\hat{\varepsilon}_x(\sigma_z) = \hat{\varepsilon}_y(\sigma_z)$, and $\varepsilon_z(\sigma_z)$ $\hat{\varepsilon}_x, \hat{\varepsilon}_y$ and through-thickness (out-of-plane) normal strain $\hat{\varepsilon}_z$. Curing stress from effective temperature: $\Delta T$ =-177˚ + 23˚ = -154˚: $\sigma_2^t = 22MPa$.

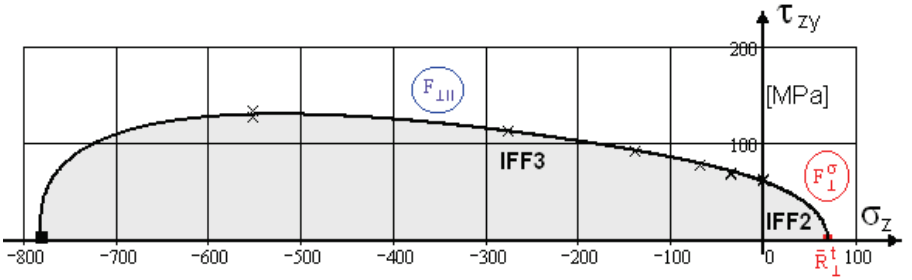


Figure 23: Applied section shear load-caused maximum-thickness failure shear stress $\tau_{zy}$ vs. applied through-thickness stress $\sigma_z$ for a $[45/\text{-}45/90/0]_{ns}$, carbon/epoxy laminate, IM7/8551-7.

Applying the data set provided for Part A the bottom curve is predicted for $\hat{\varepsilon}_z$ using $E_\perp = 8400MPa$. As can be seen a large discrepancy would remain.

The course of the Part B test data could be well mapped after studying the physical situation with increasing pressure. At first a linear situation for this well-designed laminate is faced. Then the filaments in thickness direction are more and more pressed on another which increases the stiffness in thickness direction. This has been modelled in Cuntze (2010b) by modifying $E_\perp$.

The computation indicates wedge failure at about $-400MPa$.

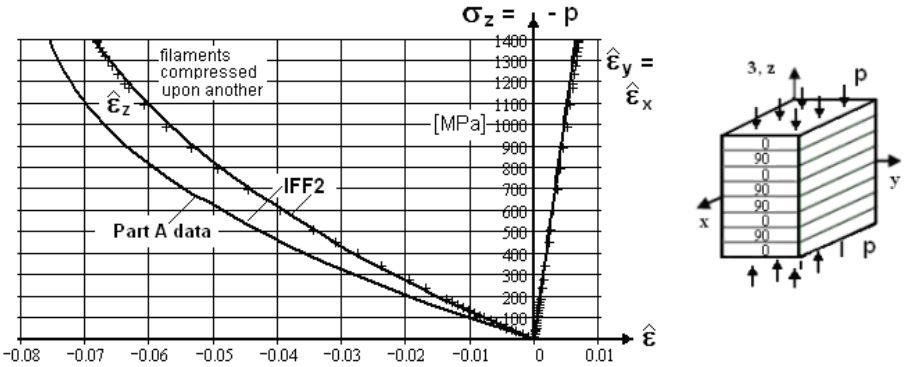


Figure 24: Single stress-strain curves caused by a through-thickness compressive stress $\sigma_z = -p$ for a $[0/90/0/90]_{ns}$ carbon/epoxy laminate, IM7/8551-7. $\sigma_x = \sigma_y = 0$. Properties as for TC10

*Lesson learnt: Squeezing of a laminate block cannot be modelled as a plain mate-*

*rial failure condition problem. One should not forget a restriction by the required design limit strain usually < 0.006. The laminate can be only re-used under thickness compression but not for general loading.*

## 8 Conclusions

***- on quality of test data Part A (prediction) and Part B***

It was very difficult for Qinetic to find reliable, well monitored test data to provide the contributors with. This task is the most challenging one of the WWFEs. An examination of several WWFE test cases is still necessary in order to satisfactorily validate a theory on the contributors side, and to judge and compare the theories of the contributing originators on the organizers side.

***- on the FMC***

- The FMC (here applied to UD material) is an efficient concept that improves and simplifies design verification. It is simply applicable to materials, if clear failure modes can be identified, and if the homogenized material element experiences a volume change or a shape change or material internal friction. It delivers a 'global' formulation of individually combined independent failure modes, without the well-known short-comings of global failure conditions which mathematically combine in-dependent failure modes.
- How well a static failure condition may be used for cyclic loading has to be established. The author presented in Cuntze (2009) his 'old' idea of a *Failure Mode-based Damage Accumulation of Brittle Materials.* Its application to UD material is *physically-based and lamina-oriented*.

***- on the application of the FMC-based UD failure conditions***

- The UD fracture failure conditions employed are proven to work in practice. The full capacity of the 3D-fracture criteria could not be fully verified. Some essential stress combinations are merely investigated or even not tested. Further, the organizers could not provide sufficient information on the IFF modes.
- In the matrix-dominated load cases the IFF have a strong influence on the stress-strain behaviour. *Final failure* occurs after the structure has degraded to a level where it is no longer capable of carrying additional load. This is most often caused by FF, however in specific cases by an IFF, too. An inclined wedge-shaped inter-fibre crack caused by IFF3 can lead to final failure if it damages the neighbouring layers by its capability to cause 3D states of stress and eventually delamination.

- P predicted initial and final non-failure envelopes did not match the test results in a number of instances. Theory was expected to give the largest discrepancy with test data in the high shear area because the computer software code developed in the present work for non-linear analysis requires further work to eliminate any convergence problems in case of high shear strains. In case of large strains the non-linear analysis has to be further improved.

- In composite laminates, composed of stiff fibres and well-designed by net theory, the fibre net controls the strain behaviour. Here, predictions are practically fully satisfying in the frame of the scatter of the design parameters.

- Usually a laminate is designed to be stable as a truss, and the laminae are stacked at angles to generate a laminate robust against possible load changes. This procedure leads to a well-designed laminate. Then the simple net theory is approximately applicable.

***- on discrepancy between theory and test***

- Main lesson learned: "Analyse your analyses with respect to input and output data and further, test your test data. Both may be worse than you think". From the applications could be learned: It's*more or less Beltrami's hypothesis + the consideration of friction all the successful FMC-conditions are based on!*

- Even in smooth stress regions a strength condition can be only a necessary condition which may be not sufficient for the prediction of 'onset of fracture', i.e. the in-situ lateral strength in an embedded lamina.

- High shear strains in practice are seldom permitted in technical applications due to operational requirements, and further do not occur in the most often used 'well-designed laminates' which are usually used in typical lightweight structures.

- Due to the higher degree of anisotropy CFRP behaves partly pretty different to GFRP.

- One should not mix up an increase of strength with an increase of resistance. Of course, both these increases lead to a reduced stress effort $E_{ff}$, that determines the *danger to fail*. However, according to Eq.(2) $E_{ff}$ may become smaller by a reduced equivalent stress $\sigma_{eq}$ and by an increased strength $R$. Both, these effects can take place under a superimposed hydrostatic stressing which – on one side - lowers $\sigma_{eq}$ and - on the other side - may improve the strength by some 'healing'.

- In case of the Test Cases with not well-designed (fibre-dominated) laminates we have to ask: What is failure? A 'limit of deformation' or 'limit of usage', is to be defined there as a functional limit. These TCs respond to generally interesting academic questions. One has to discriminate, always: What does practice need and what is of scientific interest?
- Sources that may lead to a discrepancy between prediction and test are collected below:
  - Errors and approximations in the theory
  - Errors in the experimental results and given material properties
  - Errors in the evaluation of the experiment and interpretation of data
  - Differences between fabricated and analysed laminate model
  - Lack of sufficient test data in some domains.
- When developing and testing a laminated structure - in order to understand remaining gaps between theory and experiment - we have always to keep in mind:
  - Experimental results can be far away from the reality like a bad theoretical model
  - Theory 'only' creates a model of the reality, experiment is 'just' one realisation of the reality. In this sense to say 'Comparison with experimental evidence' in Hinton et al. (2004) is very dangerous. Unfortunately in this paper some conclusions and assessments of the correlations theory-test, performed by the theory originators are not accurate. A test is not always an experimental evidence, for instance if it is not correctly interpreted (TCs in WWFE-I and –II) or evaluated or performed or ...
  - How meaningful is the scatter of test data for mapping and thereby for modelling?

*As an originator of a theory with some test experience I would like to conclude:*

***To obtain reliable test results is a bigger challenge than developing a theory.***

***Remarks:*** *The complete development of the FMC theory and the participation in the WWFEs were very effortful, non-funded elaborations of the author.*

## References

**Beltrami E.** (1885): Sulle Condizioni di Resistenza dei Corpi Elastici. *Rend. ist. d. sci. lett.,Cl. mat. nat.* 18, 705-714.

**Cuntze R.G., Deska R., Szelinski B., Jeltsch-Fricker R., Meckbach S., Huybrechts D., Kopp J., Kroll L., Gollwitzer S., Rackwitz R.** (1997): Neue Bruchkriterien und Festigkeitsnachweise für uni-direktionalen Faserkunststoffverbund unter mehrachsiger Beanspruchung –Modellbildung und Experimente–. VDI-Fortschrittbericht, Reihe 5, Nr. 506, 250 pages. In German. (New fracture criteria (Hashin-Puck action plane criteria) and Strength Design Verifications' for Unidirectional FRPs subjected to Mult-iaxial States of Stress –Model development and experiments-).

**Cuntze R.G.** (2004): Non-linear Failure Analysis of FRP Laminates composed of UD laminae -A comparison of the author's predictions with test results within the world-wide Failure Exercise in the UK-. FDM, Paderborn 2003. Trans.Tech. Publication.

**Cuntze R.G., Freund A.** (2004): *The Predictive Capability of Failure Mode Concept-based Strength Criteria for Multidirectional Laminates*. Elsevier, Part A. Composites Science and Technology 64, 343-377; (WWFE-I).

**Cuntze R.G** (2004): *The Predictive Capability of Failure Mode Concept-based Strength Criteria for Multidirectional Laminates*. Elsevier, Part B., Composites Science and Techn. 64, 487-516; (WWFE-I).

**Cuntze R.G.** (2006): Efficient 3D and 2D Failure Conditions for UD Laminae and their Application within the Verification of the Laminate Design. Elsevier, *Composites Science and Technology* 66, 1081-1096.

**Cuntze R.G.** (2007): Prediction of Static and In-plane Fracture Failure of UD Laminae composed of Fibre-reinforced Plastics. $4^{th}$ NAFEMS Nordic Seminar on Material's Modelling. Sandvika, March 2007, Conference CD.

**Cuntze R.G.** (2007): Prediction of 3D Fracture Failure of UD Laminae - visualization of failure surfaces and Mohr-Coulomb relationships. FDM07.

**Cuntze R.G.** (2008): Strength Failure Conditions of the Various Structural Materials: Is there some Common Basis existing?. FDM07, Tech. Science Press, *SDHM*, vol.074, no.1, pp.1-19.

**Cuntze R.G.** (2009): Lifetime Prediction for Structural Components made from Composite Materials – industrial view and one idea -. NAFEMS World Congress 2009, Crete, Conference paper.

**Cuntze R.G.** (2010): The Predictive Capability of Failure Mode Concept-based Strength Conditions for Laminates composed of UD Laminae under Static Triaxial Stress States. Elsevier, Part A. Composites Science and Technology, to be published; (WWFE-II).

**Cuntze R.G.** (2010): The Predictive: Capability of Failure Mode Concept - based Strength Conditions for Laminates composed of UD laminas under a Static Tri-axial State of Stress - correlation between theoretical prediction and experimental data -. Elsevier, Part B., Composites Science and Techn. (2010), to be published; (WWFE-II)

**Fischer O.** (2003): Zum Faserbruchgeschehen in Einzelschichten aus unidirektional kohlenstofffaserver-stärktem Kunststoff (on the fracture behaviour in UD CFRP laminae). Rheinisch-Westfälische Technische Hochschule Aachen, Dissertation, 2003, ISBN 3-86130-483-X

**Flaggs, D.L., Kural, M.H.** (1982): Experimental Determination of the In Situ Transverse Lamina Strength in Graphite Epoxy Laminates. *J. Comp. Mat.* vol 16, s. 103-116.

**German Guideline, Sheet 3** (2006): Development of Fibre-Reinforced Plastic Components, Analysis. (in German and English). Beuth Verlag. Author was convenor and co-author).

**Hashin Z.** (1980): Failure Criteria for Unidirectional Fibre Composites. *J. of Appl. Mech.* 47, 329-334.

**Hinton M.J., Soden P.D., Kaddour A.S.** (2004): Failure criteria in fibre reinforced polymer composites: The World-Wide Failure Exercise. Elsevier 2004 (ISBN: 0-08-044475-X), 700 pages; (WWFE-I).

**Hinton M.J., Kaddour A.S. and Soden P.M.** (2004): A further assessment of the predictive capabilities of current failure theories for composite laminates: comparison with experimental evidence. Elsevier, *Composites Science and Techn.* 64, 549-588, (WWFE-I).

**Hinton, M.J., Kaddour, A.S.** (2010): Tri-axial Test Results for Fibre-Reinforced Composites-Second World-Wide Failure Exercise Benchmark Data. Information.

**Kaddour, A.S., Hinton, M.J.** (2007):Instruction to Contributors of the Second World-Wide Failure Exercise (WWFE-II) , Part A.

**Knops M.** (2003): Sukzessives Bruchgeschehen in Faserverbundlaminaten (successive fracture behaviour of FRP laminates). Rheinisch-Westfälische Technische Hochschule Aachen, Dissertation, ISBN 3-86130-480-5.

**Leguillon D.** (2002): Strength or Toughness? –A criterion for crack onset at a notch. *Europ. J. of Mechanics A/Solids* 21, 61 - 72.

**Masters J.** (1994): *Fractography of Modern Engineering Materials.* Composites and Metals. 2nd volume. ASTM STP1203.

**Puck A.** (1996): *Festigkeitsanalyse von Faser-Matrix-Laminaten - Modelle für die Praxis* -. München: Carl Hanser Verlag.

**Puck A., Schuermann H.** (2002): Failure Analysis of FRP Laminates by Means of Physically based Phenomenological Models. Composites Science and Technology 62, 1633-1662.

**Rackwitz R., Cuntze R.G.** (1987): System Reliability Aspects in Composite Structures. *Eng.' Opt.*, Vol. 11, pp. 69-76.

**Tsai S.W., Wu E.M.** (1972): *A General Theory of Strength for An-isotropic Materials*. *Journal of Composite Materials* 5; pp.58-80.